Study of intermittent small-scale turbulence in Wendelstein 7-AS plasmas during controlled confinement transitions

N. P. Basse[a)]
Plasma Science and Fusion Center, Massachusetts Institute of Technology, Cambridge, Massachusetts 02139

S. Zoletnik
CAT-Science Bt., Detrekö u. 1/b, H-1022 Budapest, Hungary and Association EURATOM-KFKI-RMKI, H-1125 Budapest, Hungary

P. K. Michelsen
Association EURATOM-Risø National Laboratory, DK-4000 Roskilde, Denmark

W7-AS Team
Association EURATOM-Max-Planck-Institut für Plasmaphysik, D-85748 Garching, Germany

Confinement transitions in the Wendelstein 7-AS stellarator [H. Renner *et al.*, Plasma Phys. Controlled Fusion **31**, 1579 (1989)] can be induced by varying either the internal plasma current or the external magnetic field. In this paper we report on experiments where closely matched confinement states (good and bad) were constructed using the latter method. Analysis using the former scheme has been reported upon previously [S. Zoletnik *et al.*, Plasma Phys. Controlled Fusion **44**, 1581 (2002)]. The electron temperature, along with the major spectral characteristics of magnetic and small-scale electron density fluctuations, changes dramatically at the transition from good to bad confinement. The fluctuation power is intermittent, and core bursts traveling in the electron diamagnetic drift (DD) direction are correlated between the bottom and top of the plasma, especially during degraded confinement. A corresponding top–bottom correlation for the edge ion DD direction turbulence feature was not found. Strong correlations are observed both between the two density fluctuation signals and between magnetic and density fluctuations in bad compared to good confinement. The correlation time of the bursts is of order 100 μs, similar to the lifetime observed during edge localized modes. © *2005 American Institute of Physics.*
[DOI: 10.1063/1.1818142]

I. INTRODUCTION

The role of plasma turbulence in confinement transitions, both induced and spontaneous, is currently being investigated in most magnetic confinement fusion devices. This paper is part of that continual effort, and focuses on externally induced confinement transitions.

It is a well known fact that confinement in the Wendelstein 7-AS (W7-AS) stellarator[1] is very sensitive to the boundary value of the rotational transform, ι_a. Here, a is the minor radius of the plasma. Optimum confinement is found in narrow ι_a windows close to (but not at) low-order rationals $\iota_a = 1/2, 1/3$, etc.[2–4] The special significance of these windows is that they are free from the otherwise densely spaced higher-order rational ι_a values.[5] Therefore it has been assumed that perturbations arising at higher-order rational surfaces enhance the electron transport. These perturbations could be either static (due to the magnetic field) or dynamic (due to turbulence or magnetohydrodynamic activity).[6,7] The investigation in this paper is a study of the changes in electron density and magnetic fluctuations associated with the varying confinement quality at different ι_a.

The diagnostics available for our analysis are Mirnov coil measurements of magnetic fluctuations[8] and collective scattering measurements of density fluctuations using an infrared light source.[9]

We present an extended analysis of discharge types previously treated in Refs. 10 and 11. The plasmas had edge rotational transforms ι_a close to $1/3$, where confinement is very sensitive to small changes in ι_a. Good (bad) stationary confinement is achieved by setting $\iota_a \sim 0.34$ (0.36) using the external magnetic field coils; the plasmas are net current free.

At the time when analysis was done for Ref. 10, correlation techniques involving magnetic and density fluctuations[12–15] had not yet been applied to these plasma types. We find that it is essential to test whether turbulence is more strongly correlated in bad than good confinement, as has been found for spontaneous confinement transitions. In Ref. 10 we focused on wave number spectra, power spectra, and the radial profile of fluctuations. Herein, we concentrate on the intermittent behavior of turbulence in similar plasmas, so our effort constitutes a continuation of the work presented in Ref. 10.

Furthermore, additional analysis tools have been developed, e.g., a method to extract the density fluctuation

[a)]Electronic mail: basse@psfc.mit.edu; URL: http://www.psfc.mit.edu/people/basse/

TABLE I. Summary of discharges analyzed.

Shot number	θ_R	Time interval (s)	ι_a	State	W_{dia} (kJ)	$U_{volume\ 2}$ (km/s)
47 941	$-9.5°$	[0.45, 0.50]	0.345	SG	11.2	2.8
47 943	$10.5°$	[0.45, 0.50]	0.345	SG	11.2	2.9
47 944	$-9.5°$	[0.45, 0.50]	0.363	SB	4.9	2.0
47 946	$10.5°$	[0.45, 0.50]	0.363	SB	5.0	2.1

speed;[15] and the correlation techniques in Sec. III D 1 have been created specifically for this paper.

The paper is organized as follows: We describe the discharges and turbulence diagnostics in Sec. II. Spectral analysis tools, fluctuation measurements and correlation calculations aimed at studying the intermittent nature of the measured turbulence are collected in Sec. III. A discussion of the results is placed in Sec. IV. Finally, our conclusions are stated in Sec. V.

II. THE EXPERIMENTS

A. Description of the discharge types

The discharges treated in this paper were all heated on-axis by 450 kW of electron cyclotron resonance heating. The central density was 8×10^{19} m^{-3} and was kept constant by feedback gas puffing. The toroidal magnetic field was 2.5 T and the vertical magnetic field was 22 mT. The net plasma current I_p was set to zero.

Four discharges will be treated, see Table I. The first two discharges display stationary good (SG) confinement and the last two stationary bad (SB) confinement. Good (bad) confinement is characterized by a high (low) electron temperature and an energy confinement time of 26 (10) ms.

Figure 1 shows wave forms of major plasma parameters. The grey semitransparent rectangle indicates the analysis time interval written in Table I. The traces in the top row show that the current was zero for the plasmas. The second row displays traces of stored energy W_{dia} and shows that $W_{dia,SG}=11.2$ kJ and $W_{dia,SB}=4.9$ kJ. The stored energy for the other two shots follows the same pattern, see Table I. The central row shows the line density. The fourth and fifth rows

display magnetic fluctuations in shot 47 941 (SG) and shot 47 944 (SB) measured using a Mirnov coil, see Sec. II B 2.

In Fig. 2 we show electron density and temperature profiles measured using a ruby laser Thomson scattering system that provides one density/temperature profile per discharge. The density profiles show that the feedback gas puffing succeeds in keeping the density constant, regardless of the confinement state. The temperature profile for SB confinement is strongly reduced compared to SG confinement.

B. Turbulence diagnostics

1. Collective light scattering

The localized turbulence scattering (LOTUS) density fluctuation diagnostic has been described in detail elsewhere.[9] We will therefore limit ourselves to a rudimentary description below.

The radiation source is a continual wave CO_2 laser yielding 20 W. A small part of the radiation is separated from the main (M) beam and frequency shifted by 40 MHz, see Fig. 3. This second beam is called the local oscillator (LO) beam. Both beams are split in two and propagated to the plasma, where two pairs of crossed M and LO beams
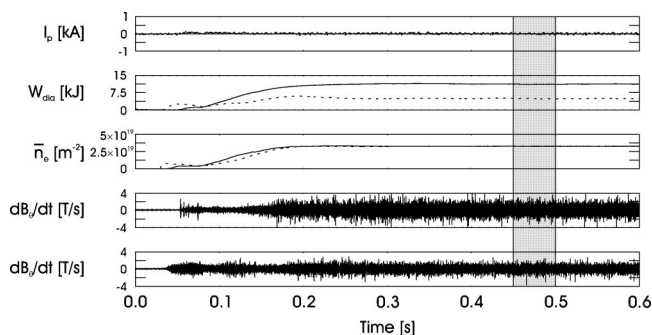

FIG. 1. Discharge overview. Shot 47 941 (SG) is represented by solid lines, shot 47 944 (SB) by dashed lines in the three top plots. From top to bottom: Plasma current, stored energy, line density, magnetic fluctuations in shot 47 941 (SG), and magnetic fluctuations in shot 47 944 (SB). The gray semitransparent rectangle indicates the analysis time interval written in Table I.
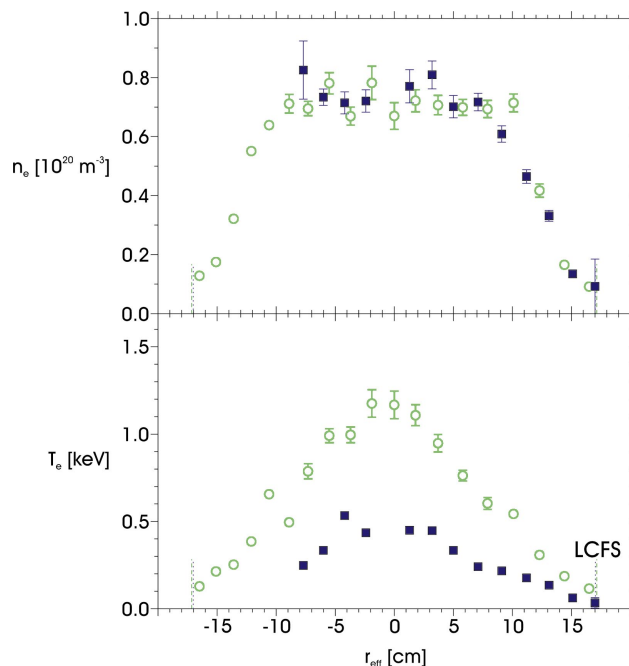

FIG. 2. (Color). Electron density (top) and temperature (bottom) profiles obtained using ruby laser Thomson scattering. Open green dots are shot 47 942 (SG) and solid blue squares are shot 47 945 (SB). The profiles are measured 400 ms into the discharges.
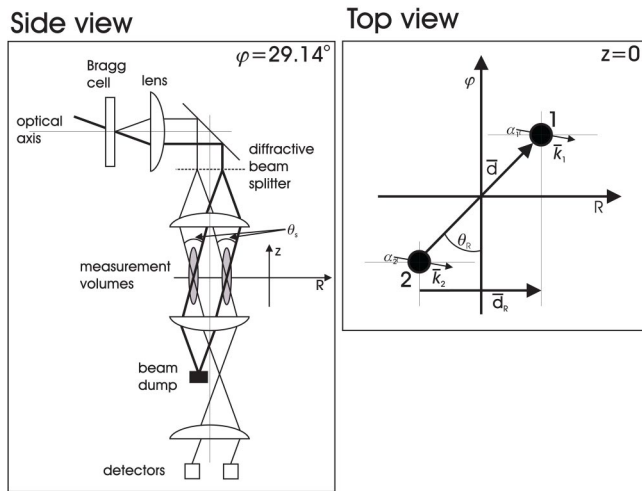
FIG. 3. Left: Schematic representation of the dual volume setup (side view). Thick lines are the M beams, thin lines the LO beams. Right: The dual volume setup seen from above. The black dots are the measurement volumes.
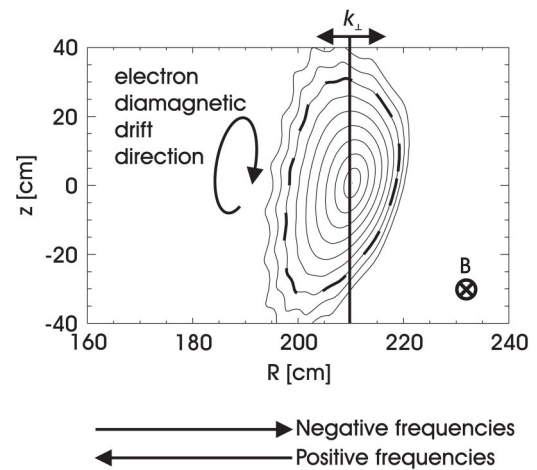

FIG. 4. Flux surfaces at the LOTUS diagnostic position. The dashed line shows the last closed flux surface (LCFS) due to limiter action. The magnetic field direction and the corresponding electron diamagnetic drift direction is indicated. The measured wave number is along the major radius R.

interfere to form the measurement volumes. The two narrow (diameter $2w = 8$ mm, where w is the beam waist) vertical measurement volumes are separated by a distance $d = 29$ mm. The measured wave number $k_\perp$ is the same in each volume and proportional to the scattering angle θ_s between the M and LO beams. In the experiments analyzed herein the direction of $k_\perp$ was set along the major radius R of the stellarator ($\alpha_1 = \alpha_2 = 0°$). For the four shots analyzed, $k_\perp$ was 15 cm^{-1}.

Aligning the angle between the measurement volumes θ_R so that the vector connecting the two measurement volumes is parallel to the local magnetic field at the top or bottom of the plasma, some spatial localization can be obtained, see, e.g., Refs. 9, 10, and 16. θ_R (which is 0° for purely toroidal separation) was set to either $-9.5°$ or 10.5°, see Table I. In our case, the angles chosen mean that we observe fluctuations localized either at the top ($\theta_R = -9.5°$) or at the bottom ($\theta_R = 10.5°$) of the plasma when we calculate the crosspower spectrum between the two volumes. The signal from a single volume (autopower) is a line integral of density fluctuations through the entire plasma column. If the crosspower between the two scattering signals is much

higher at one θ_R alignment angle than at the other, then the autopower at that frequency is dominated by a signal from the region of the plasma (top or bottom) where θ_R matches the magnetic field direction. If the crosspower at some frequency is comparable for both angles, then the source of that frequency fluctuation cannot be localized.

The vertical line in Fig. 4 indicates the position of the measurement volumes with respect to the flux surfaces. The crossing M and LO beams forming the measurement volumes are frequency shifted. Therefore heterodyne detection is performed, meaning that we can distinguish the direction of the fluctuations as being due to inward (outward) [positive (negative) frequencies] traveling fluctuations parallel to R.

2. Mirnov coil systems

W7-AS is equipped with several Mirnov coil arrays to detect fluctuations in the poloidal magnetic field B_θ. For our correlation analysis we use data acquired by the Mirnov time (MIRTIM) monitor coil; it is sampled at 250 kHz.[8] The MIRTIM coil is situated at the outboard midplane roughly
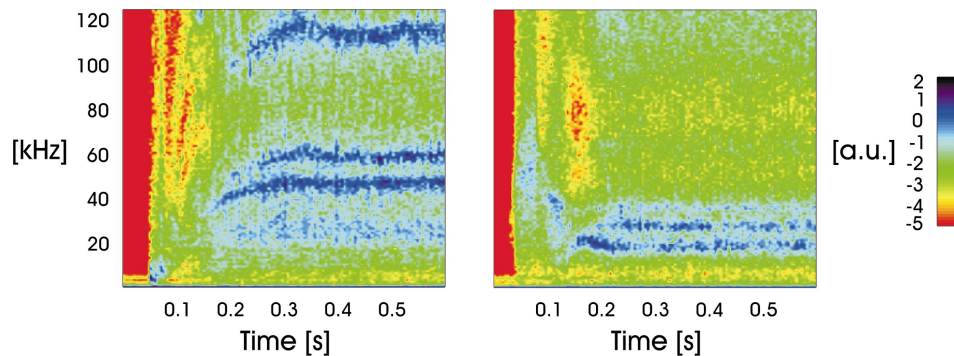

FIG. 5. (Color). Spectrograms of MIRTIM monitor coil measurements. Left, shot 47 941 (SG); right, shot 47 944 (SB), see Fig. 1. The colorscale is logarithmic.

8 cm from the last closed flux surface (LCFS). It is sensitive to fluctuations having a wave number of about 0.2 cm^{-1} and dominated by edge turbulence.[13]

In Fig. 5 we show Mirnov coil measurements of fluctuations in shots 47 941 (SG) and 47 944 (SB). During SG confinement, four separate modes can be observed from 20 to 110 kHz. In SB confinement the three low frequency modes have moved toward each other (and to lower frequencies) while the highest frequency mode is not visible.

III. TURBULENCE MEASUREMENTS

A. Spectral analysis tools

1. Autopower

The real signals acquired from each detector are centered at the heterodyne carrier frequency of 40 MHz. These are quadrature demodulated to obtain complex signals centered at zero frequency. The resulting signals are denoted

$$S_j(t) = X_j(t) + iY_j(t) = A_j(t) \times e^{i\Phi_j(t)}, \tag{1}$$

where j is the volume number (1 or 2). We can proceed and calculate

$$P_j(\nu) = \left| \int_{t_1}^{t_2} S_j(t) e^{i2\pi\nu t} dt \right|^2, \tag{2}$$

the autopower spectrum of volume j for a time interval $T = t_2 - t_1$. The autopower in a certain frequency band $\Delta\nu = \nu_2 - \nu_1$,

$$P_j^b = \int_{\nu_1}^{\nu_2} P_j(\nu) d\nu \tag{3}$$

is called the band autopower, as indicated by the lowercase superscript b in Eq. (3).

2. Crosspower

The crosspower spectrum is defined to be

$$P_{12}(\nu) = F_1^*(\nu) F_2(\nu)$$
$$= \left(\int_{t_1}^{t_2} S_1(t) e^{i2\pi\nu t} dt \right)^* \left(\int_{t_1}^{t_2} S_2(t) e^{i2\pi\nu t} dt \right), \tag{4}$$

for a time interval T.[17] The crosspower spectrum is a complex number; the amplitude and phase are called the crosspower amplitude and phase, respectively.

Usually one averages in frequency from the original $\delta\nu = 1/T_s$ of the fast Fourier transform (T_s is the original sample length, 50 ns), to some $\Delta\nu$ value, typically of order 10–100 kHz. If the actual sample length is 10 ms, this means that we average over $M = \Delta\nu/\delta\nu = 100$–1000 points in the spectrum. The power in uncorrelated parts of the spectrum is reduced due to phase mixing by a factor $\sqrt{M} = 10$–30.[9,18] Contributions to the remaining spectrum are due to correlated signals, the power being proportional to the power of the correlated fluctuations.

To understand the significance of the crosspower phase, we will assume that the signal in one volume is delayed by Δ_t relative to the signal in the other volume:

$$S_2(t) = S_1(t - \Delta_t). \tag{5}$$

This means that

$$\begin{aligned} F_2(\nu) &= \int_{t_1}^{t_2} S_2(t) e^{i2\pi\nu t} dt \\ &= \int_{t_1}^{t_2} S_1(t - \Delta_t) e^{i2\pi\nu t} dt \\ &= e^{i2\pi\nu\Delta_t} \int_{t_1}^{t_2} S_1(t - \Delta_t) e^{i2\pi\nu(t-\Delta_t)} dt \\ &= e^{i2\pi\nu\Delta_t} \int_{t_1-\Delta_t}^{t_2-\Delta_t} S_1(u) e^{i2\pi\nu u} du \approx e^{i2\pi\nu\Delta_t} F_1(\nu). \end{aligned} \tag{6}$$

The crosspower spectrum then becomes

$$P_{12}(\nu) = F_1^*(\nu) F_2(\nu) \approx F_1^*(\nu) e^{i2\pi\nu\Delta_t} F_1(\nu) = e^{i2\pi\nu\Delta_t} P_1(\nu). \tag{7}$$

The crosspower phase is here

$$\phi_{12} = 2\pi\nu\Delta_t + \phi_0 = \omega\Delta_t + \phi_0, \tag{8}$$

where we have added a constant ϕ_0; due to the optical setup, the crosspower phase is not zero at 0 Hz. The slope of the crosspower phase is equal to the time delay:

$$\frac{\partial\phi_{12}}{\partial\omega} = \Delta_t. \tag{9}$$

If there is no crosspower phase delay ($\Delta_t = 0$) but still a crosspower amplitude above noise level, this means that the structure overlaps both volumes.[19]

If there is a time delay, the group velocity of the fluctuations is $v_g = \mathcal{D}/\Delta_t$, $\mathcal{D}$ being the distance between the two measurement volumes along the group velocity vector.

3. Correlations

The cross covariance between two time series x and y is given as

$$R_{xy}(\tau) = \frac{1}{N} \sum_{k=0}^{N-|\tau|-1} (x_{k+|\tau|} - \bar{x})(y_k - \bar{y}) \text{ for } \tau < 0, \tag{10}$$

$$R_{xy}(\tau) = \frac{1}{N} \sum_{k=0}^{N-\tau-1} (x_k - \bar{x})(y_{k+\tau} - \bar{y}) \text{ for } \tau \geq 0,$$

where τ is time lag and N is the size of the two series.[18] Similarly, the cross correlation is conventionally defined in terms of cross covariances as

$$C_{xy}(\tau) = \frac{R_{xy}(\tau)}{\sqrt{R_{xx}(0) \times R_{yy}(0)}}. \tag{11}$$

In this paper we do not analyze correlations between the measured signals themselves, but we intend to investigate the correlation between the modulation of their power or band autopower, see Eq. (3). Our technique is similar to the one introduced in Refs. 20 and 21, it is fundamentally different from the standard signal correlation. This correlation calcu-
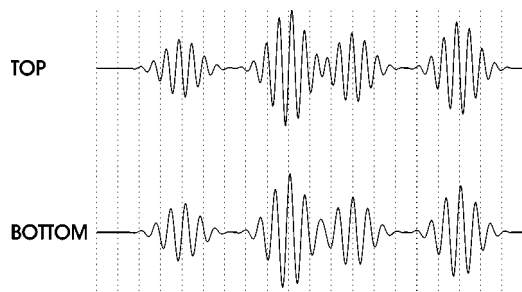
FIG. 6. Illustration of band autopower correlation between signals. The frequency of the signal at the plasma top is slightly different from the frequency at the bottom, but their amplitude is modulated in a completely correlated way. These two signals exhibit zero correlation (due to their different frequencies) but display high band autopower correlation. The signals are only for illustration of concepts, not from the measurements.

lation can be done between band autopower signals at different frequencies as illustrated in Fig. 6. If it can be shown that the signals in some frequency bands are dominated by the signal from a certain plasma region or phenomenon, the band autopower correlation technique enables the analysis of the correlation between fluctuation power at different locations or among various phenomena. Additionally the temporal correlation of band autopower signals gives information on intermittency, that is, the temporal variation of the fluctuation power.

B. Line integrated density fluctuations

In Fig. 7, we show autopower spectra of the density fluctuations in two of the discharges treated. The solid line is for SG confinement and the dashed line is for SB confinement. The good confinement state is characterized by several features: A broad, low amplitude feature at high positive frequencies and two counter propagating low frequency, high amplitude features. In bad confinement these features occupy a reduced frequency range; their amplitudes also increase markedly. The low amplitude, high positive frequency feature seems to have almost disappeared in SB confinement, but can still be discerned by a change of slope at about 800 kHz.
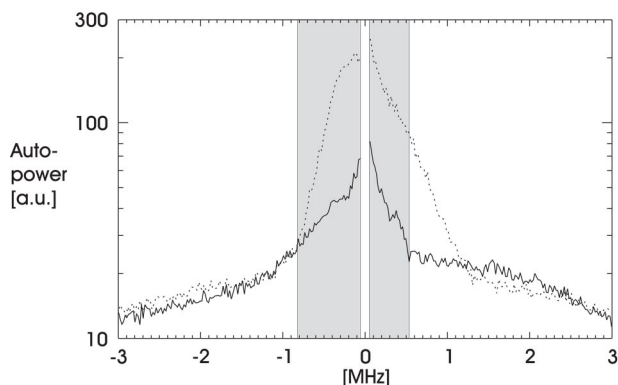

FIG. 7. Autopower spectra, volume 2. Shot 47 941 (SG) is represented by the solid line, shot 479 44 (SB) by the dashed line. The counter propagating low frequency, high amplitude features are marked by gray semitransparent rectangles.
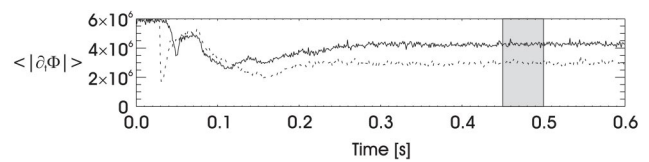

FIG. 8. Average of the absolute value of the phase derivative vs time, shots 47 941 (SG, solid line) and 47 944 (SB, dashed line). The measurements are from volume 2, the time resolution is 1 ms, and the data have been band pass filtered between 50 kHz and 3 MHz. The gray semitransparent rectangle indicates the analysis time interval written in Table I.

The reduction in frequency range from good to bad confinement implies that the speed U (magnitude of the poloidal velocity **U**) of the density fluctuations decreases. This can be quantified by calculating the derivative of the measured phase with respect to time [$\partial_t \Phi$, see Eq. (1)].[15,22] In Ref. 15, this technique was applied to plasmas in low (L) and high (H) confinement mode. In Fig. 8 we show $\langle |\partial_t \Phi| \rangle$ vs time for shots 47 941 (SG) and 47 944 (SB). Here, $\langle \cdot \rangle$ denotes a temporal average. Since $\langle |\partial_t \Phi| \rangle = k_\perp U$, where $k_\perp$ is the measured wave number, we can calculate the speed of the dominating fluctuations from the measured absolute value of the phase derivative. For the SG shots we get $U_{SG} = 2.8 \vee 2.9$ km/s and for the SB discharges we obtain $U_{SB} = 2.0 \vee 2.1$ km/s, see Table I.

A comparable behavior of the velocity a few centimeters inside the LCFS was found in Ref. 23. Both the velocity of density fluctuations calculated from the Doppler shift of reflectometry measurements and the $\mathbf{E} \times \mathbf{B}$ velocity calculated from passive spectroscopic measurements of boron IV show that the velocity decreases from good to bad confinement. Further, it was demonstrated that these density fluctuations travel in the electron diamagnetic drift (DD) direction.

Note that the autopower spectra presented in this section are not spatially localized; the crosspower spectra in Sec. III C will yield information on the structures localized at the top and bottom of the plasma.

C. Spatially localized density fluctuations

We have previously demonstrated that some spatial localization can be obtained by calculating the crosspower spectrum between two spatially separated, narrow measurement volumes.[9,10]

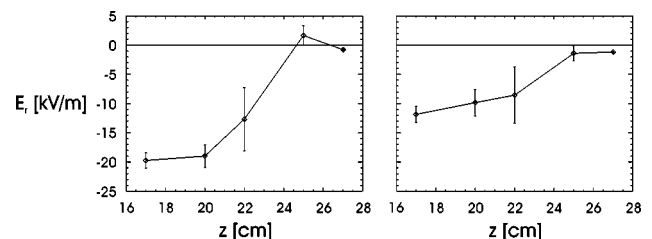Crosspower amplitudes for discharges 47 943 (SG) and 47 946 (SB) are shown in Fig. 10. The measurements are

FIG. 9. Edge radial electric field E_r as determined by boron IV spectroscopy vs z. The diagnostic coordinate z is roughly double the minor radius value. Left, shot 45 237 (SG); right, shot 45 239 (SB).
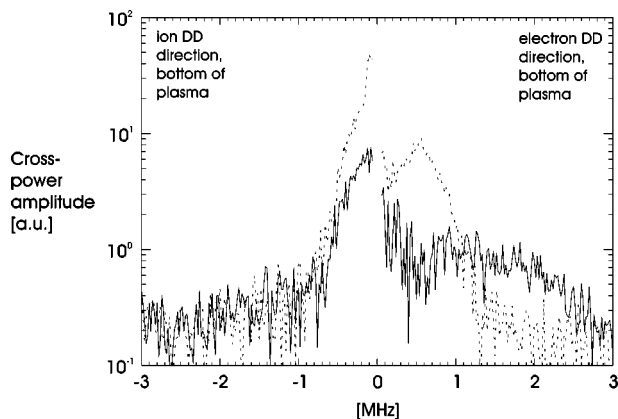
FIG. 10. Crosspower amplitude spectra at the bottom of the plasma, shots 47 943 (SG, solid line) and 47 946 (SB, dashed line).

FIG. 11. Crosspower phase spectra at the bottom of the plasma. Top, shot 47 943 (SG), bottom, shot 47 946 (SB).

localized at the bottom of the plasma; this means that fluctuations associated with positive (negative) frequencies travel in the electron (ion) DD direction.

Two features exist in SG confinement: A low frequency, high amplitude feature traveling in the ion DD direction and a high frequency, low amplitude feature traveling in the electron DD direction.[9,10] Assuming that the frequency shift of the fluctuations is dominated by the $\mathbf{E} \times \mathbf{B}$ Doppler shift, the electron feature is localized inside the LCFS, associated with the negative radial electric field (E_r) there, see Fig. 9. Conversely, the ion feature lives outside the LCFS where E_r is positive. In W7-AS, the sign of E_r generally reverses at the LCFS. The amplitude of both features increases in SB confinement, and the frequency range inhabited by the electron feature is reduced. The electron feature peaks away from dc in both good and bad confinement, in contrast to the ion feature which has its maximum close to dc.

As explained in Sec. III A 2, the slope of the crosspower phase is a measure of the time delay Δ_t between the two measurement volumes. In Fig. 11, the top plot shows the crosspower phase vs frequency for SG confinement. The bottom plot shows the crosspower phase for SB confinement. The plots show correlated fluctuations at the bottom of the plasma. In both cases, the phase displays a slope for both the ion and electron DD feature, indicating a time delay between the measurement volumes. A positive (negative) slope means that the signal in volume 2 (1) is delayed relative to the signal in volume 1 (2). Since the slopes at negative and posi-
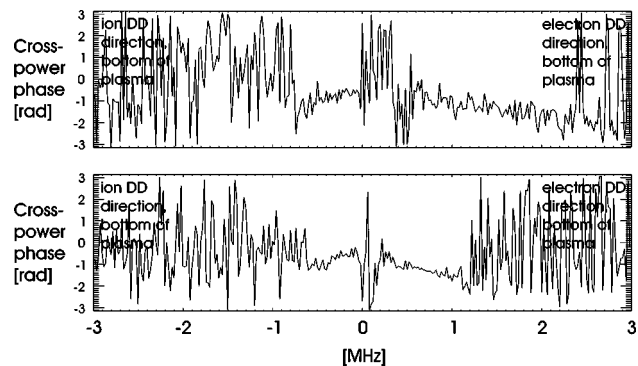
tive frequencies have opposite signs, these features are counter propagating as has already been assumed (see Fig. 10). The frequency range where a slope is visible (i.e., the frequency range where the crosspower amplitude is above the noise) is much larger for the electron compared to the ion feature, especially during good confinement. It is also clear that the frequency interval of the electron feature decreases in going from good to bad confinement.

To arrive at a more quantitative understanding of how the time delays between the volumes vary as a function of confinement quality, we made linear fits to the crosspower phases shown in Fig. 11 and corresponding measurements from the top of the plasma. The resulting delays, Δ_t, are shown in Table II. The frequency intervals in which the linear fits were made, Δ_f, are also given. These intervals were chosen by hand in each case to ensure a good quality of the fits.

The electron DD delay at the top of the plasma increases 38% from good to bad confinement ($0.24 - 0.33$ μs) and 80% ($0.10 - 0.18$ μs) at the bottom of the plasma. The larger changes of the delay at the bottom of the plasma corroborates our previous observations that the frequency range occupied by the electron DD feature changes more dramatically at the bottom than at the top of the plasma. Further, the absolute values of the time delays are largest at the top of the plasma, indicating smaller velocities.

The situation for the ion DD delays is not as clear-cut. At the top it decreases 31% ($0.32 - 0.22$ μs) and at the bottom it increases 58% ($0.19 - 0.30$ μs). The ambiguity is not under-

TABLE II. Summary of time delays between the measurement volumes.

Shot number	Plasma position	State	Direction	Δ_f (kHz)	Δ_t (μs)
47 941	Top	SG	e DD	[−1400, −400]	0.24
47 944	Top	SB	e DD	[−900, −100]	0.33
47 941	Top	SG	i DD	[0, 500]	0.32
47 944	Top	SB	i DD	[100, 500]	0.22
47 943	Bottom	SG	e DD	[500, 2300]	0.10
47 946	Bottom	SB	e DD	[300, 1200]	0.18
47 943	Bottom	SG	i DD	[−700, −100]	0.19
47 946	Bottom	SB	i DD	[−500, −100]	0.30

stood; the ion feature is associated with the positive E_r outside the LCFS. So the opposing trends are localized in the scrape-off layer (SOL) at the very top and bottom of the plasma.

D. Intermittency

In this section we investigate whether the amplitude of density and magnetic field fluctuations is constant in time or intermittent. The analysis is done by calculating band autopower signals defined by Eq. (3) and analyzing the correlation between different frequencies.[20,21,24] As was discussed in the previous sections, different frequency ranges correspond to different features and to different locations in the plasma, therefore a correlation analysis between different frequencies reveals information on the correlation of different turbulent features.

The amplitude of the scattered signal might be modulated by various mechanisms.

(1) Statistics of the observed scattering events (waves, perturbations) in the plasma. This arises from the finite number of events seen by the diagnostic at a given time. A modulation of this type would not mean that the turbulence is intermittent.

(2) Noise associated with the diagnostic. As was shown in Ref. 9, the dominant noise source in the LOTUS diagnostic is white detector noise, so it would not introduce a correlation between band autopower signals measured in different volumes and/or at different frequencies. On the other hand this component will contribute to the magnitude of the cross correlation defined by Eq. (11).

(3) Intermittent modulation of the turbulence in the plasma. We are interested in this modulation, since it might reveal information on the turbulence mechanism itself.

These sources of modulation can be distinguished by analyzing the spatial, temporal, and frequency range of the correlations. To ensure that modulations are not caused by some phenomenon specific to the laser scattering diagnostic, correlations between band autopowers and the rms amplitude of Mirnov coil signals are also presented.

1. Correlations in the modulation of density fluctuation power

In this section, we will investigate cross correlations [see Eq. (11)] between different band autopowers [see Eq. (3)], i.e., temporal changes of the density fluctuation power at different frequencies. A comparison of the crosspower spectra between volumes aligned along the magnetic field at the bottom and the top of the plasma reveals (see Fig. 14 in Ref. 10) that above about 500 kHz the autopower spectra are dominated by scattering from the bottom (positive frequencies) or top (negative frequencies). This allows us to correlate the power modulation of fluctuations at the bottom and top of the plasma by correlating band autopower signals at high negative and positive frequencies. A correlation between the modulation of the power at negative and positive frequencies would either mean that (i) the waves observed by LOTUS travel from the top to the bottom (and/or from the bottom to the top) of the plasma poloidally along a flux
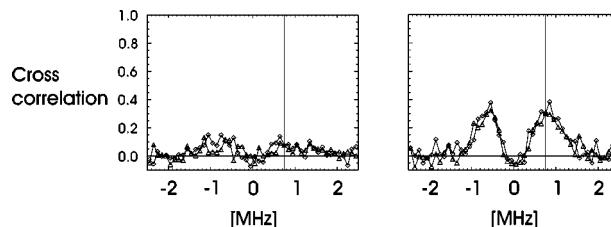

FIG. 12. Left, shot 47 941 (SG); right, shot 47 944 (SB). Diamonds: Cross correlation at zero time lag between reference band autopower [700, 800] kHz, volume 2 and band autopowers in volume 1. Triangles: Cross correlations with the volumes switched. The vertical lines mark the reference frequency.

surface or that (ii) some mechanism modulates the density fluctuation power at the top and bottom of the plasma in a correlated way. As was shown in Ref. 9, the cross-field correlation length $\mathcal{L}_\perp$ of the fluctuations is of order 1 cm, so mechanism (i) can be excluded. This means that by analyzing the correlation between negative and positive frequencies we are studying a phenomenon which modulates the fluctuation power and not the fluctuations themselves.

We will initially let the band autopower from 700 to 800 kHz be the reference signal [y series in Eq. (11)], and correlate this signal with band autopowers in the other volume, ranging from −2.5 to 2.5 MHz [x series in Eq. (11)]. The time resolution is 100 μs. The correlations are made both using volume 1 and volume 2 as reference signals. However, this does not affect the results.

Figure 12 shows the cross correlation at zero time lag vs frequency for shot 47 941 (SG) and 47 944 (SB). Correlations corresponding to those shown have also been calculated for time lags away from zero. This investigation established that the correlation has a maximum at zero time lag, and decreases symmetrically for both positive and negative time lags, see Fig. 13. First of all it is clear that whether one uses volume 1 (triangles) or volume 2 (diamonds) as a reference, the result is the same.

During SG confinement, a low level of correlation is observed, but remains below about 10%. In contrast, the SB confinement correlations are quite large, up to 40%. The correlation peak at positive frequencies is wider than the negative frequency one.

We interpret this "double-hump" correlation as follows: The fluctuations in the reference band are correlated with fluctuations in the other volume having both the same and the opposite frequency sign. This situation arises because the
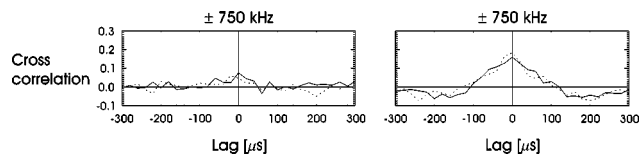

FIG. 13. Cross correlation between density fluctuation band autopowers vs time lag (units of 20 μs). Left, cross correlation for shot 47 941 (SG); right, cross correlation for shot 47 944 (SB). Solid lines are the cross correlations between the [700, 800] kHz band autopowers in volume 1 and the [−800, −700] kHz band autopowers in volume 2. Dashed lines: Cross correlations with the volumes switched.
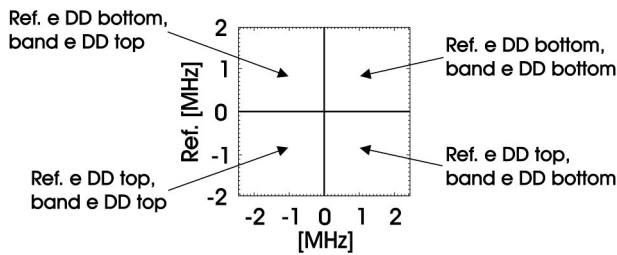
FIG. 14. We assume that the correlations observed in Fig. 12 are due to fluctuations traveling in the electron DD direction. Combining this with the conventions of Fig. 4, we conclude that correlations in each quadrant of the grid shown originate from different fluctuation components.
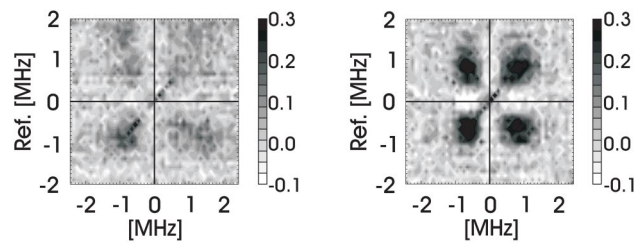

FIG. 15. Left, shot 47 941 (SG); right, shot 47 944 (SB). Cross correlation between reference band autopowers, volume 2, and band autopowers in volume 1. The contour plots are displayed vs reference and band frequency.

fluctuation power at the bottom and top of the plasma is being modulated simultaneously. We have seen that the correlated fluctuations are generally restricted to rather high frequencies (above a few hundred kilohertz). Since we know that the ion (electron) DD feature exists at low (high) frequencies, the correlated fluctuations are traveling in the electron DD direction. In the present case, this means that the reference band is observing electron DD fluctuations at the bottom of the plasma, see Fig. 4. The correlation hill at positive (negative) frequencies is due to correlated fluctuations in the other volume traveling in the electron DD direction at the bottom (top) of the plasma. That explains our observation made above that the positive frequency peak is wider than the one for negative frequencies.

It is interesting that the correlations seen in Fig. 12 do not extend to low frequencies. This means that the low frequency ion DD feature [which resides outside the LCFS (Ref. 10)] is not correlated with the high frequency electron DD feature inside the LCFS. Similar observations that SOL turbulence is disconnected from core fluctuations have been published in, e.g., Ref. 25.

Let us return to Fig. 13: We define the correlation time to be the full width at half maximum (FWHM) of the cross correlation function. We let positive (negative) frequency band autopowers be the x (y) series in Eq. (11). This means that for positive lags, positive frequency fluctuations occur first, while for negative lags, they are delayed with respect to the negative frequency turbulence. No clear correlation is observed for SG confinement, but a correlation is seen for SB confinement with a correlation time of about 100 μs. The cross correlation maximum amplitude is reduced to 20% from 40% for the corresponding point in the right-hand plot of Fig. 12 (at −750 kHz) because of the increased time resolution from 100 to 20 μs. So the reduction in the cross correlation is due to the reduced signal-to-noise ratio arising from the binning of fewer measurement points. There is no peak in the cross correlation function away from zero time lag, which strengthens our conclusion that the correlations measured are due to mechanism (ii), see the first paragraph in this section.

The next step in our analysis of correlated fluctuations in the two volumes is to calculate correlations using a wide range of reference frequencies: −2 to 2 MHz (100 kHz bandwidth, 100 μs time resolution). With the help of Fig. 4, we can understand the meaning of contour plots having ref-

erence band autopowers [y series in Eq. (11)] on one axis and band autopowers [x series in Eq. (11)] on the other. In Fig. 14, we see that correlations in each quadrant have different meanings in terms of localization.

Now that we have established the interpretation of this type of contour plots, we proceed to the measurements.

The left-hand plot of Fig. 15 shows correlations for SG confinement: A localized, modest correlation in the lower left-hand quadrant, and a smaller, broader correlation in the upper right-hand quadrant. The broad (narrow) correlation originates at the bottom (top) of the plasma. The mixed top-bottom correlations are rather broad and have small amplitudes.

The right-hand plot of Fig. 15 shows correlations for SB confinement. Here, we see that each quadrant has an "island" of strongly correlated high frequency fluctuations. If we compare the upper right-hand and lower left-hand quadrant, we find what would be expected: The bottom correlation extends to higher frequencies than the top one, since the frequency of the electron DD feature is highest at the bottom. The amplitude of the correlation is largest at the top, as is the case for the crosspower amplitude. Correlations in the two other quadrants—due to a combination of fluctuations at the top and bottom of the plasma—have similar amplitudes.

For both SG and SB confinement a "stripe" of low frequencies is correlated between the two volumes. This is a real effect; correlations calculated using 20 ms of background data (no plasma) do not exhibit any systematic structure at all, see Fig. 16. So the stripe is caused by ion DD fluctuations correlated between the two volumes at the top (upper right-hand quadrant) and bottom (lower left-hand quadrant) of the plasma. However, no correlation is seen between the top and the bottom of the plasma, therefore this
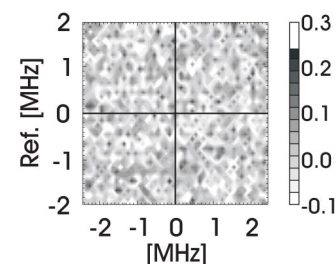

FIG. 16. Shot 47 941 (SG), background data: Cross correlation between reference band autopowers, volume 2, and band autopowers in volume 1. The contour plot is displayed vs reference and band frequency.
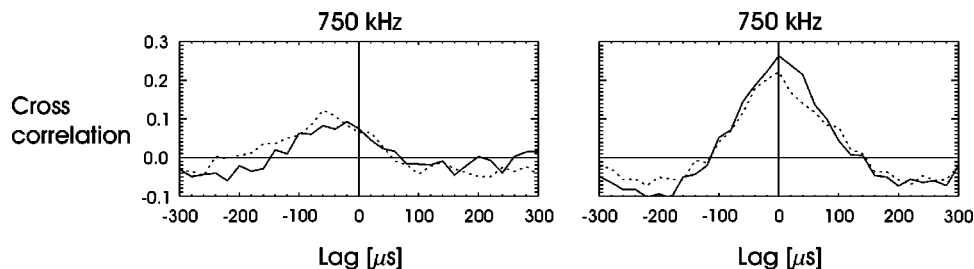
FIG. 17. Cross correlation between magnetic and density fluctuations vs time lag (units of 20 μs). Left, cross correlation for shot 47 941 (SG); right, cross correlation for shot 47 944 (SB). Solid line is volume 1, dashed line volume 2.

observation might simply arise due to the statistics of turbulent events in the SOL. For SG confinement the ion feature is only seen at the top of the plasma. During SB confinement the ion feature is top-bottom symmetric and has a lower frequency.

2. Correlations between the modulation of density and magnetic fluctuation power

We now turn to correlations between band autopowers and magnetic fluctuations. We will let the band autopower of the density fluctuations be the x series, and y be the rms power of the Mirnov coil signal, see Eq. (11) and Ref. 13. This means that for positive lags, density fluctuations occur first, while for negative lags, they are delayed with respect to the Mirnov coil series.

If a correlation is detected, it does not mean that the density fluctuations observed by laser scattering have a magnetic component. The laser scattering measures millimeter-scale structures, while the Mirnov coil signals are sensitive only to several centimeter-scale structures. A correlation would therefore simply mean that some event occurs in the plasma which modulates the amplitude of *both* magnetic and density fluctuations.

Figure 17 shows the cross correlation between density fluctuations in the [700, 800] kHz frequency band and magnetic fluctuations for shots 47 941 and 47 944. The left-hand plot is for SG confinement and the right-hand plot is for SB confinement. A weak correlation (up to 10%) is visible for SG confinement, centered at a time lag of -50 μs; this means that the magnetic fluctuations occur 50 μs before the density fluctuations. The SB confinement correlation is symmetric around zero time lag and has a maximum correlation of 30%. The correlation time in the SB confinement case is about 100 μs, comparable to the result displayed in Fig. 13.

We show contour plots of the correlations between magnetic and density fluctuations in Fig. 18. Time lag is shown on the vertical axis, up to ±300 μs in steps of 20 μs. The time lags are shown vs density fluctuation band frequency in volume 2 (100 kHz bandwidth).

The SG confinement shot has correlations centered at zero time lag for frequencies in the range [-1400, -300] kHz. In contrast, the correlations at positive frequencies peak for different values of the time lag: At high frequencies (2 MHz), the time lag is zero, as opposed to low frequencies (500 kHz), where the time lag is -50 μs, see the left-hand plot in Fig. 17.

The SB confinement correlations are centered at zero time lag: The range of the negative (positive) frequency correlations is [-1300, -300] ([300, 1300]) kHz. Their amplitudes are much larger than those found in SG confinement.

The correlations in both SG and SB confinement are for fluctuations traveling in the electron DD direction. The negative (positive) frequency correlations are at the top (bottom) of the plasma. The positive frequency range is largest, since the electron DD feature has higher frequencies at the bottom than at the top of the plasma.

It is worth noting that no correlation is observed at low frequencies, that is, for the power of the ion DD feature. This agrees well with the earlier observation,[25] that SOL turbulence is purely electrostatic, therefore no magnetic fluctuation is involved.

IV. DISCUSSION

A. Confinement and correlated fluctuations

The general observation that the transition from bad to good confinement is associated with a decreased level of correlated fluctuations has also been found for the L-H transition.[12–15] Correlations during bad confinement seen in the present paper are not due to edge localized modes (ELMs), but are probably caused by "ELM-like" transport events.[25,26] Proper ELMs and H modes are only observed in W7-AS with the t_a value in certain operational windows.[27] The fact that the correlations we have discovered for bad confinement are akin to those identified in L mode suggests that the term ELM-like is a good label for these turbulent bursts. However, it is not clear to what extent the observed increase in intermittency (correlation of band autopower signals) in bad confinement is due to the increase in fluctuation amplitude or due to stronger intermittency, but the tendency fits into the idea that the presence of ELM-like events is
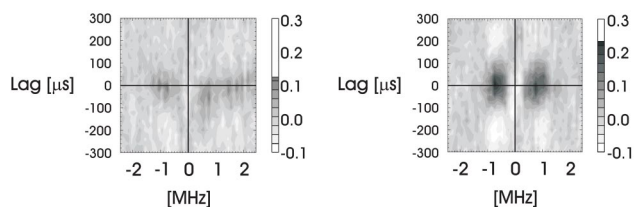

FIG. 18. Cross correlation between Mirnov rms signal and density fluctuation band autopower (volume 2) vs band frequency and time lag (units of 20 μs). Left, shot 47 941 (SG); right, shot 47 944 (SB).

associated with a worsening of global confinement. ELM-like events are not as localized at the edge as proper ELMs, which usually occur 2–3 cm inside the LCFS. However, one can make the statement that ELM-like events are localized roughly at the maximum of the pressure gradient.[28]

Within the last couple of years, a multitude of observations have been published indicating the existence of zonal flows (ZF), see, e.g., Refs. 29–32. Our observations in Sec. III D 1 that the fluctuation band autopower is instantaneously correlated at the bottom and top of the plasma also seem to indicate a global ($n=0, m=0$) ZF structure. In future work we will pursue this question by investigating low frequency modulations of the density fluctuation velocity. This will be done both by analyzing the crosspower phase and the speed of density fluctuations. If a low frequency geodesic acoustic mode (GAM) is causing the observed correlations, this should be reflected in high frequency fluctuations.[31,33]

B. Confinement and the radial electric field

In studies of density fluctuations during L and H mode we found that the average L- (H-) mode speed of the density fluctuations was 600 (400) m/s, see Refs. 13 and 15. In that case, improved confinement was associated with a reduction of the speed of the fluctuations.

In the present case, for confinement transitions created by varying t_a, we discovered the opposite tendency: The average speed of the density fluctuations in bad (good) confinement was found to be 2 (3) km/s.

The cause of these differences, both in the trend and magnitude of the speed, is most likely due to the behavior of E_r. For edge profiles of E_r, see Refs. 13 and 15 (L and H mode) and Refs. 12 and 23 (good to bad confinement transition). We will concentrate on the description of the discharges treated in this paper and refer to Refs. 13 and 15 for the analysis of L- and H-mode E_r measurements.

If the speed of density fluctuations is dominated by $\mathbf{E} \times \mathbf{B}$ rotation effects, the speeds found correspond to radial electric fields of −5 kV/m (bad confinement) and −7.5 kV/m (good confinement). This is in agreement with E_r measurements from a few centimeters inside the LCFS, see Secs. III B and III C.

There is definitely a larger E_r shear in the edge plasma for good confinement compared to bad confinement, see Fig. 9. Further, as we have seen above, the amplitude of E_r at the radial position where the density fluctuations occur is largest for good confinement. This means that the fluctuations are rotating faster in the poloidal direction during good confinement. These observations are consistent with turbulence suppression in good confinement due to E_r shear.[34,35]

Faster rotation during good confinement fits the general trend found in Sec. III C that electron DD time delays between the two LOTUS volumes are smallest for good confinement.

V. CONCLUSIONS

We have presented an analysis of fluctuations in plasmas exhibiting good and bad confinement. Stationary good and bad confinement plasmas were created using the external coils exclusively to modify the edge rotational transform.

We have analyzed the intermittency (modulation) of density fluctuation power and found that the electron DD core plasma feature is modulated at the bottom and top of the plasma in a correlated way. As turbulent structures are known to travel only some centimeters in the poloidal direction, this observation indicates that the fluctuation amplitude is modulated on an entire flux surface. It is not yet clear whether this modulation causes local profile flattenings (ELM-like phenomena) or if it is simply a consequence of the flattening by some other phenomena. In the latter case, small-scale turbulence phenomena would just monitor the ELM-like events. It is important to note that for the edge ion DD feature this top-bottom correlation was not observed.

Correlations between magnetic and density fluctuations confirmed the analysis performed using only density fluctuation measurements. The correlation time of the bursts is of order 100 μs, similar to the lifetime observed during edge localized modes. A comparable correlation time was found correlating Mirnov coil band autopowers in Ref. 36. It is possible that the correlated fluctuations are due to large-scale zonal flows; that is a topic for future work.

A new line of investigation is whether the behavior of turbulence in this type of confinement transition can be reproduced in tokamaks. Similarity experiments in the Alcator *C*-Mod tokamak have been initiated to answer this question.[37] Here, the plasma current is ramped to vary the edge safety factor q_a around 3 where we would expect a transition analogous to the one found in W7-AS.

[1] H. Renner, W7AS Team, NBI Group, ICF Group, and ECRH Group, Plasma Phys. Controlled Fusion **31**, 1579 (1989).
[2] R. Jaenicke, E. Ascasibar, P. Grigull *et al.*, Nucl. Fusion **33**, 687 (1993).
[3] R. Brakel, M. Anton, J. Baldzuhn *et al.*, Plasma Phys. Controlled Fusion **39**, B273 (1997).
[4] R. Brakel, M. Anton, J. Chatenet *et al.*, in *Proceedings of the 25th EPS Conference on Controlled Fusion and Plasma Physics*, ECA (European Physical Society, Petit-Lancy, 1998), Vol. 22C, p. 423.
[5] H. Wobig, H. Maassberg, H. Renner *et al.*, in *Proceedings of the 11th IAEA Conference on Fusion Energy* (International Atomic Energy Agency, Vienna, 1986), Vol. 2, p. 369.
[6] R. Brakel, M. Anton, V. Erckmann *et al.*, J. Plasma Fusion Res. **1**, 80 (1998).
[7] R. Brakel and W7-AS Team, Nucl. Fusion **42**, 903 (2002).
[8] M. Anton, R. Jaenicke, A. Weller *et al.*, in *Proceedings of the 24th EPS Conference on Controlled Fusion and Plasma Physics*, ECA (European Physical Society, Petit-Lancy, 1997), Vol. 21A, p. 1581.
[9] M. Saffman, S. Zoletnik, N. P. Basse *et al.*, Rev. Sci. Instrum. **72**, 2579 (2001).

[10] S. Zoletnik, N. P. Basse, M. Saffman *et al.*, Plasma Phys. Controlled Fusion **44**, 1581 (2002).

[11] N. P. Basse, P. K. Michelsen, S. Zoletnik *et al.*, Plasma Sources Sci. Technol. **11**, A138 (2002).

[12] N. P. Basse, Ph.D. thesis, University of Copenhagen, 2002, http://www.risoe.dk/rispubl/ofd/ris-r-1355.htm

[13] N. P. Basse, S. Zoletnik, M. Saffman *et al.*, Phys. Plasmas **9**, 3035 (2002).

[14] N. P. Basse, S. Zoletnik, S. Bäumel *et al.*, Nucl. Fusion **43**, 40 (2003).

[15] N. P. Basse, S. Zoletnik, G. Y. Antar *et al.*, Plasma Phys. Controlled Fusion **45**, 439 (2003).

[16] N. P. Basse, S. Zoletnik, and P. K. Michelsen, Phys. Scr. (to be published).

[17] E. J. Powers, Nucl. Fusion **14**, 749 (1974).

[18] J. S. Bendat and A. G. Piersol, *Random Data: Analysis and Measurement Procedures* (Wiley, New York, 2000).

[19] D. Grésillon, C. Stern, A. Hémon *et al.*, Phys. Scr. **T2/2**, 459 (1982).

[20] F. J. Crossley, P. Uddholm, P. Duncan *et al.*, Plasma Phys. Controlled Fusion **34**, 235 (1992).

[21] P. J. Duncan and M. G. Rusbridge, Plasma Phys. Controlled Fusion **35**, 825 (1993).

[22] G. Antar, P. Devynck, C. Laviron *et al.*, Plasma Phys. Controlled Fusion **41**, 733 (1999).

[23] M. Hirsch, E. Holzhauer, J. Baldzuhn *et al.*, Plasma Phys. Controlled Fusion **43**, 1641 (2001).

[24] T. Dudok de Wit, in *The URSI Review on Radio Science 1993–1995*, edited by R. E. Stone (Oxford University Press, Oxford, 1996).

[25] S. Zoletnik, M. Anton, M. Endler *et al.*, Phys. Plasmas **6**, 4239 (1999).

[26] M. Hirsch, M. Anton, J. Baldzuhn *et al.*, in *Proceedings of the 25th EPS Conference on Controlled Fusion and Plasma Physics*, ECA (European Physical Society, Petit-Lancy, 1998), Vol. 22C, p. 2322.

[27] M. Hirsch, P. Grigull, H. Wobig *et al.*, Plasma Phys. Controlled Fusion **42**, A231 (2000).

[28] M. Hirsch (private communication).

[29] S. Coda, M. Porkolab, and K. H. Burrell, Phys. Rev. Lett. **86**, 4835 (2001).

[30] M. Jakubowski, R. J. Fonck, and G. R. McKee, Phys. Rev. Lett. **89**, 265003 (2002).

[31] G. R. McKee, R. J. Fonck, M. Jakubowski *et al.*, Phys. Plasmas **10**, 1712 (2003).

[32] G. S. Xu, B. N. Wan, M. Song *et al.*, Phys. Rev. Lett. **91**, 125001 (2003).

[33] G. R. McKee, R. J. Fonck, M. Jakubowski *et al.*, Plasma Phys. Controlled Fusion **45**, A477 (2003).

[34] B. Lehnert, Phys. Fluids **9**, 1367 (1966).

[35] H. Biglari, P. H. Diamond, and P. W. Terry, Phys. Fluids B **2**, 1 (1990).

[36] G. Pokol, G. Por, S. Zoletnik *et al.*, in *Proceedings of the 30th EPS Conference on Controlled Fusion and Plasma Physics*, ECA (European Physical Society, Petit-Lancy, 2003), Vol. 27A, p. P-3.7.

[37] N. P. Basse, E. M. Edlund, C. L. Fiore *et al.*, in *Proceedings of the 31st EPS Conference on Controlled Fusion and Plasma Physics*, ECA (European Physical Society, Petit-Lancy, 2004), Vol. 28B, p. P-2.161.